

Biophysical Journal

**Supporting Material**

**Hysteresis in the cell response to time-dependent substrate stiffness**

Achim Besser and Ulrich S. Schwarz

## I. DESCRIPTION OF MODEL EQUATIONS

The complete mechano-chemical model has been described previously [1]. In the following we briefly review all model equations, summarized in Tab. SI. We start with a description of the reaction diffusion equations for the Rho-pathway, that is initiated at focal adhesions. We then discuss the mechanical stress fiber equation and how the biochemical signal couples into its contraction dynamics.

**Eq. (m1):** It is expected that mechanical forces exerted on focal adhesions eventually initiate the GTP loading of RhoA leading to the activation of the Rho associated kinase (ROCK). Due to the lack of information we lump the focal adhesion associated processes into one equation that effectively describes the conversion of ROCK into its activated form (presumably complexed with RhoA-GTP). The mechanical force  $F_t$  that stimulates the activation is treated as an enzyme in the framework of Michaelis-Menten kinetics. The variable ROCK in Eq. (m1) denotes the activated form of ROCK and we assume that the overall concentration of ROCK is constant at  $\text{ROCK}_{\text{tot}}$ . The force exerted by the stress fiber on the focal adhesion,  $F_t(t)$ , stimulates the conversion of ROCK into its activated form with maximum velocity  $r_1 F_t(t)$  and Michaelis-Menten constant  $K_1$ . The parameter  $r_1$  is equivalent to a rate constant but relates mechanical force to a chemical reaction. For this reason the units of  $r_1$  are given as [nM/s nN], see Tab. SII. The second term accounts for the degradation of activated ROCK to its inactive form, with maximum velocity  $V_{-1}$  and Michaelis-Menten constant  $K_{-1}$ . Since we expect ROCK in its active form to be associated with focal adhesions, we omit diffusive contributions to this equation.

**Eq. (m2) and (m3):** One main effector of ROCK is myosin light chain phosphatase (MLCP), which we regard as a diffusible compound, described by the reaction-diffusion equation. Here, the variables MLCP-P and MLCP denote the phosphorylated and unphosphorylated form of myosin light chain phosphatase, respectively. The first term accounts for the dephosphorylation of MLCP-P with maximum velocity  $V_{-2}$  and Michaelis-Menten constant  $K_{-2}$ . The second term allows for the diffusion of the phosphatase with diffusion constant  $D$ . The phosphorylation level of MLCP is also regulated by the active form of ROCK which catalyzes the reverse reaction, that is the conversion of the phosphatase into its phosphorylated form. ROCK is only active in the vicinity of focal adhesions located at each end of the stress fiber. Thus, this source term can be incorporated into the boundary conditions for Eq. (m2). The diffusive flux into the boundary has to balance the conversion into its inactive form, see Eq. (bc2) in Tab. SI. The reaction at the boundaries is again modeled by Michaelis-Menten kinetics, where  $R_2 = r_2 v_b$  is the product of a rate constant  $r_2$

with an effective volume  $v_b$  of the focal adhesion in which the reaction takes place.  $K_2$  is the usual Michaelis-Menten constant. An equivalent reaction-diffusion equation with the same boundary conditions follows for the phosphorylated form of the phosphatase (MLCP-P), see Eq. (m3) and Eq. (bc3) in Tab. SI.

**Eq. (m4):** MLCP together with myosin light chain kinase (MLCK) regulate the phosphorylation level of myosin light chain (MLC). Since myosin in stress fibers form mini-filaments, which are bound to actin filaments, we neglect diffusion of this compound, leading to the rate equation for the phosphorylated fraction  $n$  of MLC. By allowing only the ratio of the phosphorylated fraction to vary, we assume that the overall amount of myosin in stress fibers is constant. MLC is phosphorylated by MLCK with a maximum velocity  $V_3 = r_3 \text{MLCK}$  and respective Michaelis-Menten constant  $K_3$ . We assume that the concentration of MLCK is constant within the cell. The kinase is antagonized by MLCP that dephosphorylates MLC with a rate constant  $r_{-3}$  and Michaelis-Menten constant  $K_{-3}$ . Since MLCP has spatial dependent source terms and is diffusible, the inhibition of MLC by the phosphatase will vary in space.

The factor  $I$  in Eq. (m4) accounts for the effect of calyculin on actomyosin contractility. Calyculin is an inhibitor of MLCP and thereby enhances the phosphorylation level of MLC. We model the interaction of calyculin with its target MLCP as a competitive inhibition [2]. The unperturbed case corresponds to  $I = 1$ . Induction of calyculin corresponds to  $I > 1$  which, in the model, effectively increases the Michaelis-Menten constant  $K_{-3}$  and thus decreases the rate of MLC dephosphorylation. Thus, more myosin motors will be activated and cell contractility is stimulated.

The used parameter values for the reaction-diffusion system are based on an extensive survey of the literature and are summarized in Tab. SII. If a range of values is reported in the literature, we chose an intermediate value for this parameter. If no value could be found in the literature, we made reasonable assumptions based on similar parameters in other systems. No attempt was made to fit the parameters to some target function.

**Eq. (m5):** The stress fiber model equation has previously been derived and discussed in detail [1, 3]. It describes the displacement  $u(x, t)$  along the fiber and is derived from the force balance of passive viscoelastic and active contractile forces:

$$a^2 \frac{\partial}{\partial x} \left( \gamma(x) \frac{\partial}{\partial x} \dot{u}(x, t) \right) + a^2 \frac{\partial}{\partial x} \left( k(x) \frac{\partial}{\partial x} u(x, t) \right) + a \frac{\partial F_m(x, t)}{\partial x} = 0 \quad (1)$$

The first and the second term represent the passive viscous and elastic forces, respectively. The frictional coefficient is given by  $\gamma$ , the elastic constant is denoted by  $k$ ,  $a$  is the typical length of a sarcomeric unit, see Tab. SII. The third term accounts for the contractile actomyosin forces. The

contraction force  $F_m$  is described by a linear force-velocity relation:  $F_m(x, t) = F_s(x, t)(1 + \frac{v(x, t)}{v_0})$  with stall force  $F_s$  and maximum motor velocity  $v_0$ . The local contraction velocity of the fiber  $v(x, t)$  is given by the local strain rate  $v(x, t) = -a\partial_x\dot{u}(x, t)$  which leads to:

$$F_m(x, t) = F_s(x, t) \left( 1 + \frac{a}{v_0} \frac{\partial}{\partial x} \dot{u}(x, t) \right) \quad (2)$$

We couple the biochemical signaling to the actomyosin contraction by assuming that the stall force depends on the phosphorylated fraction  $n(x, t)$  of MLC along the stress fiber. This assumption is based on the fact that myosin heads can only bind to actin and perform an ATP-cycles if MLC is phosphorylated. The more myosin heads are activated along a myosin minifilament, the larger the maximum force that the bundle can exert to the actin filaments. Thus, we regard the ensemble of myosins within a cross section of a stress fiber as one large contractile unit with an effective stall force that depends linearly on the active fraction  $n$  of myosin heads:

$$F_s(x, t) = F_{max} n(x, t) \quad (3)$$

The effective stall force  $F_s(x, t)$  would reach the maximum force  $F_{max}$  if all myosins within this cross section were activated ( $n = 1$ ). Eq. (1) together with Eq. (2) and Eq. (3) lead to the final stress fiber model given by Eq. (m5). The boundary conditions at the two ends of the fiber (each end is terminating at one focal adhesion) are given by a balance of the stress fiber forces, namely the traction forces  $F_t$ , and the elastic restoring forces from the compliant substrate. The latter is modeled as linear elastic spring of stiffness  $k_s$ . The boundary conditions are given in Eq. (bc5).

## II. ANALYSIS OF SUBSTRATE DEFORMATION

Instead of the traction force  $F_t$  one could also choose the substrate deformation  $u$  as a state variable in the bifurcation analysis. The analysis is equivalent in the sense that these two measures are linearly related by  $F_t = |k_s u|$ . Nevertheless, the bifurcation diagram for the substrate deformation reveals some notable features which we want to discuss here. The bifurcation diagram is shown Fig. S1 for different values of the stimulation strength  $I$ . The upper stable branch exhibits a maximum at an intermediate stiffness ratio. This is because on the one hand the contractile forces sharply decrease with decreasing substrate stiffness as the left bifurcation point is approached, compare Fig. 2 in the main text. Thus, also the resulting deformations decrease in the vicinity of the left bifurcation point. On the other hand, the exerted forces saturate for large stiffness ratios. As a consequence, the deformations roughly decay proportional to  $1/k_s$  for high stiffness ratios.

These results depict the dilemma experimentalists face when they perform experiments with cells on soft substrates and measure the resulting substrate deformations. On a very stiff substrate, cells are able to build up high forces, but since the substrate is so stiff, the caused displacements are very small and hardly measurable. On the other hand, if the substrate is very soft, cells can not exert large forces, thus the substrate deformations are also very small and hardly measurable. There is only a small window of suitable substrate stiffness over which cells reach a contractile state and the substrate is sufficiently soft to allow for measurable deformations.

We have also analyzed the time courses of the substrate deformations when substrates of cyclic stiffness are imposed. The sinusoidal function of the time-dependent substrate stiffness was, as in the main text, given by:

$$k_s(t)/k = 10^{-2} + 10 \left( \frac{1}{2} + \frac{1}{2} \cos(\omega t) \right) \quad (4)$$

The results for the substrate deformations are shown in Fig. S2. The same periods have been used in the main text. Also here, the area of the hysteresis cycle first increases with the angular frequency, reaches a maximum (not necessarily at the same  $T$ -value as the force) and then decreases again with increasing frequency. In the latter case, when the frequency is very high, the system maintains unusually high forces on soft substrates. This combination of high forces and low stiffness leads to very large deformations. This can be deduced from the trajectories for  $T < 4300$  s which undergo large excursions away from the steady state branches. It is also noteworthy that the substrate deformations reach a maximum shortly before the stiffness passes through its minimal value.

### III. BUILD UP OF TRACTION FORCES

To simulate the build up of traction forces during cell spreading we imposed that initially all biochemical components are equilibrated for vanishing mechanical input. That is, we have set  $F_t(t) = 0$  in Eq. (m1) and let the biochemical components evolve to their steady state. The resulting concentration profiles are then taken as initial conditions for the subsequent simulation. This situation is meant to represent a cell that was formerly in suspension where no forces could be built up and that starts to adhere to the substrate at  $t = 0$ . The time courses of the established traction forces on substrates of different stiffness are shown in Fig. S3. We find that the stiffer the substrate the faster is the build up of contractility and the higher is the force reached in the steady state. However, the reached steady state forces of cells in the contractile state only differ within a few percent, reflecting the fact that eventually all motors are activated and loaded to their stall

force. A dramatically simplified version (the so-called *two-spring model*) of this process has been analyzed before [4]. As discussed earlier, cells on very soft substrates, (see  $k_s/k = 0.46$  in Fig. S3), can not establish high traction forces and are kept in the inactive state.

#### IV. DISCUSSION OF CONTROL PARAMETERS

To perform the stability analysis of our model, we have chosen the non-dimensional ratio of substrate stiffness over stress fiber stiffness  $k_s/k$  and the stimulation strength  $I$  (calyculin) as control parameters of the model system because both can be directly addressed by well established experimental methods. All other model parameters have been given a specific value based on literature reports. However, it is important to note that the bistability results from the inherent positive feedback in the system and is not constraint to variations in a specific model parameter. For this reason, the control parameter  $I$  can also be exchanged by another reaction parameter and the model still remains bistable, as we have verified explicitly for some selected parameters.

- 
1. Besser, A., and U. S. Schwarz, 2007. Coupling biochemistry and mechanics in cell adhesion: A model for inhomogeneous stress fiber contraction. *New Journal of Physics* 9:425.
  2. Klipp, E., R. Herwig, A. Kowald, C. Wierling, and H. Lehrach, 2005. Systems biology in practice. concepts, implementation and application. Wiley-VCH, Berlin.
  3. Colombelli, J., A. Besser, H. Kress, E. G. Reynaud, P. Girard, E. Caussinus, U. Haselmann, J. V. Small, U. S. Schwarz, and E. H. K. Stelzer, 2009. Mechanosensing in actin stress fibers revealed by a close correlation between force and protein localization. *Journal of Cell Science* 122:1665–1679.
  4. Schwarz, U. S., T. Erdmann, and I. B. Bischofs, 2006. Focal adhesions as mechanosensors: The two-spring model. *BioSystems* 83:225–232.
  5. Feng, J., M. Ito, Y. Kureishi, K. Ichikawa, M. Amano, N. Isaka, K. Okawa, A. Iwamatsu, K. Kaibuchi, D. J. Hartshorne, and T. Nakano, 1999. Rho-associated kinase of chicken gizzard smooth muscle. *Journal of Biological Chemistry* 274:3744–3752.
  6. Hartshorne, D. J., M. Ito, and F. Erdoedi, 1998. Myosin light chain phosphatase: Subunit composition, interactions and regulation. *Journal of Muscle Research and Cell Motility* 19:325–341.
  7. Nagamoto, H., and K. Yagi, 1984. Properties of myosin light chain kinase prepared from rabbit skeletal muscle by an improved method. *Journal of Biochemistry* 95:1119–1130.
  8. Butler, T. M., S. R. Narayan, S. U. Mooers, and M. J. Siegman, 1994. Rapid turnover of myosin light chain phosphate during cross-bridge cycling in smooth muscle. *American Journal of Physiology- Cell Physiology* 267:C1160–1166.

9. Amano, M., M. Ito, K. Kimura, Y. Fukata, K. Chihara, T. Nakano, Y. Matsuura, and K. Kaibuchi, 1996. Phosphorylation and activation of myosin by Rho-associated kinase (Rho-kinase). *Journal of Biological Chemistry* 271:20246–20249.
10. Hathaway, D. R., and R. S. Adelstein, 1979. Human platelet myosin light chain kinase requires the calcium-binding protein calmodulin for activity. *Proceedings of the National Academy of Sciences* 76:1653–1657.
11. Nunnally, M. H., S. B. Rybicki, and J. T. Stull, 1985. Characterization of chicken skeletal muscle myosin light chain kinase. Evidence for muscle-specific isozymes. *Journal of Biological Chemistry* 260:1020–1026.
12. Bartelt, D. C., S. Moroney, and D. J. Wolff, 1987. Purification, characterization and substrate specificity of calmodulin-dependent myosin light-chain kinase from bovine brain. *Biochemical Journal* 247:747–756.
13. Pato, M. D., and R. S. Adelstein, 1983. Purification and characterization of a multisubunit phosphatase from turkey gizzard smooth muscle. The effect of calmodulin binding to myosin light chain kinase on dephosphorylation. *Journal of Biological Chemistry* 258:7047–7054.
14. Lippincott-Schwartz, J., E. Snapp, and A. Kenworthy, 2001. Studying protein dynamics in living cells. *Nature Reviews. Molecular Cell Biology* 2:444–456.
15. Balaban, N. Q., U. S. Schwarz, D. Riveline, P. Goichberg, G. Tzur, I. Sabanay, D. Mahalu, S. Safran, A. Bershadsky, L. Addadi, and B. Geiger, 2001. Force and focal adhesion assembly: A close relationship studied using elastic micro-patterned substrates. *Nature Cell Biology* 3:466–472.
16. Umemoto, S., and J. R. Sellers, 1990. Characterization of in vitro motility assays using smooth muscle and cytoplasmic myosins. *Journal of Biological Chemistry* 265:14864–14869.
17. Peterson, L. J., Z. Rajfur, A. S. Maddox, C. D. Freel, Y. Chen, M. Edlund, C. Otey, and K. Burridge, 2004. Simultaneous stretching and contraction of stress fibers in vivo. *Molecular Biology of the Cell* 15:3497–3508.
18. Deguchi, S., T. Ohashi, and M. Sato, 2006. Tensile properties of single stress fibers isolated from cultured vascular smooth muscle cells. *Journal of Biomechanics* 39:2603–2610.
19. Kumar, S., I. Z. Maxwell, A. Heisterkamp, T. R. Polte, T. P. Lele, M. Salanga, E. Mazur, and D. E. Ingber, 2006. Viscoelastic retraction of single living stress fibers and its impact on cell shape, cytoskeletal organization, and extracellular matrix mechanics. *Biophysical Journal* 90:3762–3773.

Model equations	
$\frac{\partial \text{ROCK}(t)}{\partial t} = \frac{r_1 F_t(t)(\text{ROCK}_{\text{tot}} - \text{ROCK}(t))}{K_1 + (\text{ROCK}_{\text{tot}} - \text{ROCK}(t))} - \frac{V_{-1} \text{ROCK}(t)}{K_{-1} + \text{ROCK}(t)}$	(m1)
$\frac{\partial \text{MLCP}(x, t)}{\partial t} = \frac{V_{-2} \text{MLCP-P}(x, t)}{K_{-2} + \text{MLCP-P}(x, t)} + D \frac{\partial^2 \text{MLCP}(x, t)}{\partial x^2}$	(m2)
$\frac{\partial \text{MLCP-P}(x, t)}{\partial t} = -\frac{V_{-2} \text{MLCP-P}(x, t)}{K_{-2} + \text{MLCP-P}(x, t)} + D_p \frac{\partial^2 \text{MLCP-P}(x, t)}{\partial x^2}$	(m3)
$\frac{\partial n(x, t)}{\partial t} = \frac{V_3 (1 - n(x, t))}{K_3 + (1 - n(x, t))} - \frac{r_{-3} \text{MLCP}(x, t) n(x, t)}{K_{-3} I + n(x, t)}$	(m4)
$a^2 \frac{\partial}{\partial x} \left( \tilde{\gamma}(x, t) \frac{\partial}{\partial x} \dot{u}(x, t) \right) + a^2 \frac{\partial}{\partial x} \left( k(x) \frac{\partial}{\partial x} u(x, t) \right) + a \frac{\partial}{\partial x} F_s(x, t) = 0$	(m5)
Boundary conditions at $x = 0, L$	
$\frac{\partial \text{MLCP}(x, t)}{\partial x} = \pm \frac{R_2}{D} \frac{\text{ROCK}(t) \text{MLCP}(x, t)}{K_2 + \text{MLCP}(x, t)}$	(bc2)
$\frac{\partial \text{MLCP-P}(x, t)}{\partial x} = \mp \frac{R_2}{D_p} \frac{\text{ROCK}(t) \text{MLCP}(x, t)}{K_2 + \text{MLCP}(x, t)}$	(bc3)
$F_t(t) = \pm k_s(t) u(x, t)$	(bc5)
Abbreviations	
$F_s(x, t) = F_{max} n(x, t)$	
$\tilde{\gamma}(x, t) = \gamma(x) + F_s(x, t)/v_0$	
$F_t(t) = a \tilde{\gamma}(x, t) \frac{\partial}{\partial x} \dot{u}(x, t) + a k(x) \frac{\partial}{\partial x} u(x, t) + \frac{\partial}{\partial x} F_s(x, t)$	

TABLE SI: Summary of model equations. Eqs. (m1-m4) describe successive biochemical signaling events: (m1) focal adhesion associated activation of ROCK; (m2) and (m3) phosphorylation and diffusion of MLCP and dephosphorylation and diffusion of MLCP-P; (m4) regulation of the active fraction of the myosins, which is identified with the phosphorylated fraction of MLC. Eq. (m5) is the model equation for stress fibers where  $u(x, t)$  is the displacement along the fiber. The boundary conditions for the partial differential Eqs. (m2), (m3), (m5) are given by (bc2), (bc3), (bc5), respectively. In Eq. (bc2), (bc3), (bc5) the upper (lower) sign is valid for the left  $x = 0$  (right  $x = L$ ) boundary. For brevity we have introduced abbreviations for the stall force  $F_s$ , the effective viscosity  $\tilde{\gamma}$  and the traction forces  $F_t$ . All presented results have been derived with the assumptions that: (I) The diffusion properties of the phosphorylated and unphosphorylated form of the phosphatase are the same, hence  $D = D_p$ . (II) The viscoelastic properties of the stress fiber do not vary in space, therefore  $k(x) \rightarrow k$  and  $\tilde{\gamma}(x, t) \rightarrow \gamma + F_{max} n(x, t)/v_0$ .

Time dependent reaction variables				
Abbreviation	Meaning	Used value	Reference values	Ref.
ROCK	activated form of ROCK	0 ... 5 nM	$\gtrsim 1$ nM	[5]
MLCP	unphosphorylated form of MLCP	0 ... 1.2 $\mu$ M	$1.2 \pm 0.3$ $\mu$ M	[6]
MLCP-P	phosphorylated form of MLCP	0 ... 1.2 $\mu$ M	$1.2 \pm 0.3$ $\mu$ M	[6]
$n$	fraction of active myosin	0 ... 1	[MLC-P]/[myosin]	
Reaction constants				
MLCK	myosin light chain kinase	0.1 $\mu$ M	$\gtrsim 100$ nM	[7]
$M$	myosin concentration	30 $\mu$ M	25 ... 30 $\mu$ M	[8]
$K_1$	Michaelis constant	5 nM	(no value)	
$K_{-1}$	Michaelis constant	7 nM	(no value)	
$K_2$	Michaelis constant	0.1 $\mu$ M	$0.10 \pm 0.01$ $\mu$ M	[5]
$K_{-2}$	Michaelis constant	15 $\mu$ M	(no value)	
$K_{3*M}$	Michaelis constant	20 $\mu$ M	$52.1 \pm 7.1$ $\mu$ M	[9]
			$34.5 \pm 2.8$ $\mu$ M	[5]
			18 $\mu$ M	[10]
			7.7 ... 96.0 $\mu$ M	[11]
			19 ... 53 $\mu$ M	[7]
			20 $\mu$ M	[12]
$K_{-3*M}$	Michaelis constant	10 $\mu$ M	10 $\mu$ M	[13]
$r_1$	rate constant	0.3 nM/s nN	(no value)	
$V_{-1}$	maximum velocity	1.7 nM/s	(no value)	
$r_2$	rate constant	2.4 1/s	$2.36 \pm 0.10$ 1/s	[5]
$R_2$	maximum velocity	4.8 $\mu$ m/s	$r_2 * v_b$	
$V_{-2}$	maximum velocity	0.1 $\mu$ M/s	(no value)	
$r_{3*M}$	rate constant	10 1/s	$2.00 \pm 0.36$ 1/s	[9]
			$3.85 \pm 0.095$ 1/s	[5]
			5.17 1/s	[10]
			7.37 ... 171.3 1/s	[11]
			70 ... 100 1/s	[7]
			4.64 1/s	[12]
$V_{3*M}$	maximum velocity	1.0 $\mu$ M/s	$r_{3*MLCK*M}$	
$r_{-3*M}$	rate constant	21 1/s	21 1/s	[13]
$D$	diff. const. of MLCP & MLCP-P	14 $\mu$ m <sup>2</sup> /s	10 ... 100 $\mu$ m <sup>2</sup> /s	[14]
$v_b$	effect. react. vol. of FAs	2.0 $\mu$ m	(no value)	
Parameters of mechanical model				
$F_{max}$	stall force	50 nN	20 ... 70 nN	[15]
$v_0$	maximum motor velocity	1.0 $\mu$ m/s	$\approx 0.1 \dots 1$ $\mu$ m/s	[16]
$a$	sarcomeric length	1.0 $\mu$ m	1.0 $\mu$ m	[17]
$k$	spring stiffness	45 nN/ $\mu$ m	$45.7$ nN/ $a$	[18]
$\gamma$	viscosity	45 nN s/ $\mu$ m	$\approx \tau k = 45.7$ nN s/ $a$	[18, 19]
$L$	fiber length	50 $\mu$ m	$\approx 20 \dots 80$ $\mu$ m	

TABLE SII: Model parameters based on literature search. We have set the model parameters such that they fit into the reported range. The equation for the phosphorylated fraction of MLC is normalized to the total myosin concentration denoted by  $M$ . In order to make the involved reaction constants comparable to the literature values we give  $K_3$ ,  $K_{-3}$ ,  $r_3$ ,  $r_{-3}$  and  $V_3$  scaled with  $M$ . The lower and higher estimates for  $F_{max}$  have been taken from traction force measurements of fibroblasts and myocytes, respectively [15]. The typical equilibration time  $\tau$  of stress fibers is a few seconds [3, 19] which yields a rough estimate for the viscosity  $\gamma \approx \tau k$ , using  $\tau = 1$  s. Some of the reported values have been measured for the interactions of protein fractions and not for the native proteins. Furthermore, the experiments have been carried out on proteins extracted from different species.

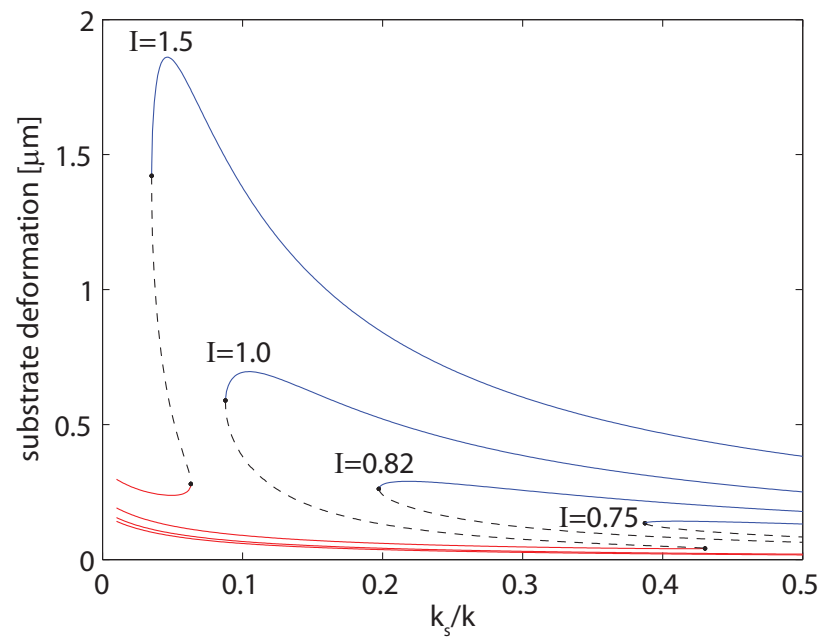


FIG. S1: (a) Bifurcation diagrams for the substrate deformations. The color coding is as in Fig. 2 in the main text.

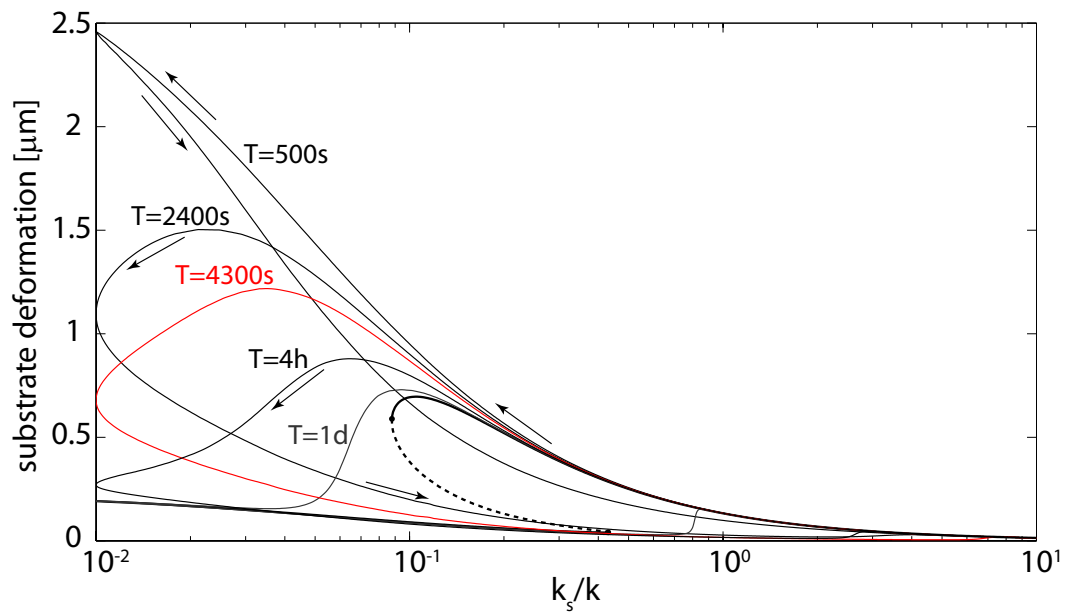


FIG. S2: Time course of the substrate deformation for a cyclic varying substrate stiffness with periods used as in the main text. The curve highlighted in red corresponds to the largest hysteresis cycle in Fig. 4 in the main text. For small periods, the substrate deformation exhibit large excursions to very high values.

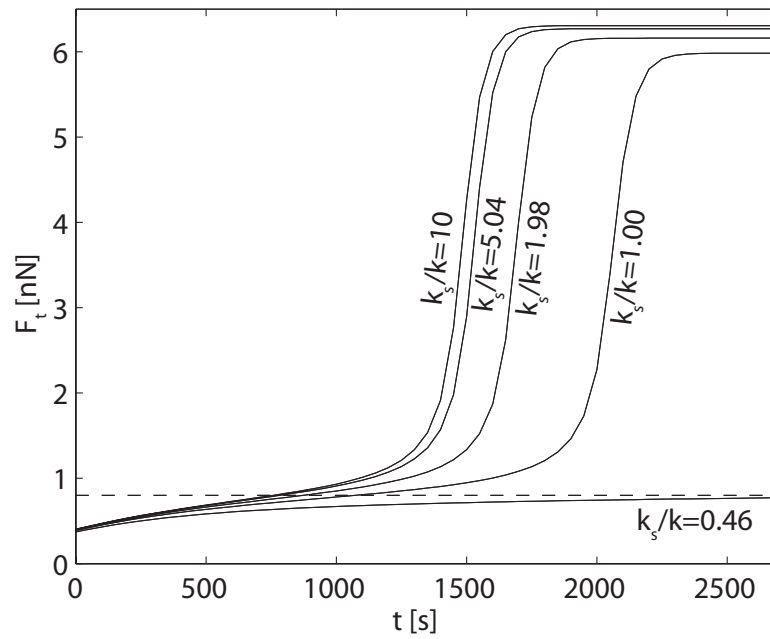


FIG. S3: Time course of the traction forces established by cells on substrates with different stiffness:  $k_s/k \in \{0.46, 1.00, 1.98, 5.04, 10\}$ . The stiffer the substrate the faster is the equilibration process and the higher is the force reached in the steady state. Cells on the softest substrate,  $k_s/k = 0.46$ , can not establish high contraction forces and are kept in the inactive state.